Structure and function of the cerebral cortex in Huntington's disease

Coppen, E.M.

7

The visual pathway in **Huntington's disease**; a diffusion tensor imaging and neurophysiological study

Emma M. Coppen, Anne Hafkemeijer,
Jeroen van der Grond, Robert H.A.M. Reijntjes,
Martijn R. Tannemaat, Raymund A.C. Roos

Submitted

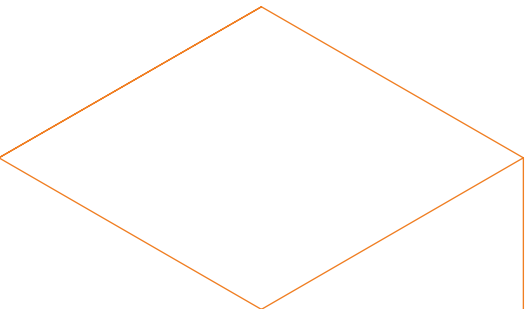

ABSTRACT

Objective: To investigate microstructure and function of the visual pathway and determine clinical correlates in Huntington's disease (HD) patients.

Methods: Diffusion tensor-imaging data was acquired of 21 premanifest, 20 manifest HD, and 17 healthy controls. To examine the microstructure of white matter pathways, mean indices of diffusion parameters were measured along the anterior and posterior thalamic radiation tracts using Tract-Based Spatial Statistics (TBSS). Additionally, electrical activity of the brain in response to visual stimuli was measured using pattern-reversal visual-evoked potentials (VEPs). Associations with clinical measures were examined in HD gene carriers using univariate linear regression analyses corrected for age, gender, and HD group.

Results*:* Microstructural alterations in manifest HD were primarily present in the optic radiations of posterior brain regions and to a lesser extent in the anterior brain regions. Reduced fractional anisotropy, and increased radial and axial diffusivity were associated with higher disease burden scores and increased oculomotor impairment in HD gene carriers. Radial diffusivity showed the strongest associations with oculomotor function and disease burden. Normal latencies of the pattern-reversal VEP were found in HD gene carriers compared to controls. Reduced amplitudes of the early components were present in premanifest HD and manifest HD, but were not associated with clinical measures.

Conclusion*:* Altered microstructure of the posterior optic radiation is detectable in early manifest HD and is related with disease severity. Our results show that axonal degeneration in the occipital lobe occurs early in the disease process, while functional integrity of the visual pathway remains relatively preserved.

1. INTRODUCTION

Huntington's disease (HD) is a hereditary, neurodegenerative disorder, characterized by a triad of progressive motor disturbances, cognitive decline and behavioral changes.[1] The disease is caused by an abnormal expansion of the CAG (cytosine-adenosine-guanine) repeat length in the Huntingtin gene on chromosome four.[2] Atrophy of the striatum is the neuropathological hallmark of the disease due to extensive loss of striatal medium-sized spiny neurons.[3] As a result, striatal atrophy is thought to be the origin of the typical unwanted choreiform movements that occur in patients with HD.[3,4] Neuroimaging studies have shown that striatal atrophy can be detected a decade before clinical disease onset in the so-called premanifest phase, and is therefore seen as a robust marker to track disease progression.[5,6] However, besides the characteristic clinical signs of HD, deficits in visual cognition, such as an impaired visuospatial working memory or changes in facial emotion recognition have been frequently reported,[7] and are suggested to originate from posterior cortical degeneration, since pronounced reductions in the absolute nerve cell number in the occipital lobe have been found in advanced HD patients.[8–10]

Moreover, in earlier disease stages, volume loss in posterior cortical brain regions is present,[11–15] and is even associated with worse visual cognitive task performance and oculomotor dysfunction.[11,12,15] It has therefore been proposed that besides striatal atrophy, cortical degeneration also contributes to the clinical phenotype of HD.[15]

Although there is increasing evidence of the involvement of posterior brain regions in the neurodegenerative process of HD, the extent of structural and functional changes of the *in-vivo* pathways to these regions remains unclear. In our study, we aimed to gain more insight into the neuropathological involvement of posterior brain regions in HD. We therefore assessed white matter diffusion properties and neurophysiological measurement of visual-evoked potentials to investigate structural and functional alterations of the visual pathway in premanifest and manifest HD gene carriers.

2. METHODS

2.1. Participants

Fifty-eight participants (21 premanifest HD gene carriers, 20 manifest HD gene carriers, and 17 healthy controls) were included in this cross-sectional, observational study via the outpatient clinic of the Neurology department at the Leiden University Medical Center (LUMC) in the Netherlands. All HD gene carriers had a genetic test with ≥ 36 CAG repeats. Spouses and HD gene-negative relatives were recruited as

controls. Participants were required to have a normal or corrected-to-normal primary visual ability above 0.5 (20/40) on the visual acuity test and no major ophthalmic or neurologic co-morbidities. Participants were not included if they were unable to undergo MRI scanning (i.e. due to metallic implants, claustrophobia, or pregnancy). Patients that participated in an intervention trial were not included in this study. The Medical Ethical Committee of the LUMC approved this study and written informed consent was obtained from all participants.

Demographic data, including gender, date of birth, age at visit, and years of education, was obtained for all participants. Primary visual acuity and the ability to perceive color differences were assessed using a visual acuity test and the Ishihara Color Test respectively. HD gene carriers were divided into premanifest and manifest HD based on the presence of motor signs using the Unified Huntington's Disease Rating Scale (UHDRS) total motor score.[16] This scale measures the degree of motor disturbances in different domains, such as oculomotor function, gait and postural stability, and the presence of choreiform or dystonic movements. A higher score indicates more motor impairments. The clinically manifest phase of the disease is defined as an UHDRS – total motor score of more than 5, whereas HD gene carriers with a score of 5 or less are defined as premanifest individuals. The ocular and saccadic movement items of the UHDRS were summed to establish a subdomain score (range 0 – 24) of oculomotor function, as described previously.[12,17] The disease burden score (age x [CAG repeat length – 35.5]) was calculated for all HD gene carriers, in which a higher score reflects an increased disease severity.[18]

2.2. DTI acquisition

Diffusion Tensor Imaging (DTI) data was acquired on a 3-Tesla whole body MRI scanning system (Philips Achieva, Best, the Netherlands) using a standard 32-channel head coil. A single shot echo-planar DTI sequence was applied with 32 gradient directions and a total acquisition time of approximately 8 minutes. The follow scan parameters were used: TR = 11.547 ms, TE = 56 ms, FOV = 220 x 220 mm^2 with an acquisition matrix of 112 x 110, 2 mm slice thickness with no gap between slices, flip angle = 90°, voxel size = 1.96 x 1.96 x 2.00 mm^3, number of slices = 75, b-value = 1000 s/mm^2, and halfscan factor = 0.61.

2.3. DTI processing

Diffusion tensor imaging data were preprocessed using the FMRIB's Diffusion Toolbox (FDT) that is implemented in FMRIB's Software Library (FSL, version 5.0.10, Oxford, United Kingdom).[19,20] First, images were corrected for distortions caused by eddy

currents and motion artifacts. Then, diffusion tensors were fit to the eddy-current corrected data resulting in fractional anisotropy (FA), radial diffusivity (RD or $\lambda\perp$) and axial diffusivity (AD or $\lambda||$) maps. RD was defined as the average of the second and third eigenvalues of the diffusion tensor ($\lambda_2 + \lambda_3 / 2$), while AD corresponded to the first eigenvalue (λ_1).

The FA, RD, and AD maps from each participant were further analyzed using voxel-wise tract-based spatial statistics (TBSS) analysis, part of FSL.[21] Here, FA images from all participants were nonlinearly registered to a standard space target image (FMRIB58_FA image) to form an averaged registered FA image. Then, a skeleton of white matter was generated by thresholding the averaged FA image, in which only voxels with a mean FA value of 0.2 or higher were included. Consequently, this mean FA skeleton represents the center of the white matter fibers throughout the whole brain. The skeleton projection was then applied to RD, and AD images, to create a separate skeleton for each diffusion measure. All data was visually checked for distortions or incorrect registration.

The anterior and posterior thalamic radiations (including the optic radiations) tracts were used as a mask of the visual pathway and mean FA, RD, and AD values within this mask were extracted. These tracts were identified using the Johns Hopkins University white matter tractography atlas implemented in FSL.

2.4. Visual-evoked potentials (VEP)

Electrical activity of the brain in response to visual stimuli was measured using a pattern-reversal VEP (Medelec Synergy, Oxford Instruments, version 11.0) at the department of Clinical Neurophysiology in the LUMC.

The left and right eyes were stimulated separately in two sessions (a total of four sessions), and were then averaged to form one trace per eye. A high-contrast full-field black-and-white checkerboard was used that flashed at a frequency of 2 Hz with an individual square check size of 0.45 degrees of arc. Participants were seated facing the checkerboard screen at a viewing distance of 2 meter in a dark room and were asked to fixate their gaze on the center of the screen with one eye covered. The EEG signal was recorded using an active mid-occipital (Oz) electrode and referenced to Cz, according to the international 10/20 system. A total of 100 trials were recorded. Trials containing artifacts were manually removed before further analyses.

Four major components (N75, P100, N140 and P200) were measured to analyze brain activity in the occipital cortex. For each component, the latency was calculated to indicate the time from stimulus onset to the component, whereas the amplitude was measured from peak to baseline (i.e. peak amplitude) and from peak to peak (i.e.

peak-to-peak amplitude), as described in the guidelines of the International Society for Clinical Electrophysiology of Vision (ISCEV).[22]

2.5. Statistics

Group differences in demographic characteristics were analyzed using analysis of variance (ANOVA), independent T-test or chi-square test when applicable. Group differences between the extracted mean FA, RD, and AD values of the white matter tracts of interest were analyzed using ANOVA with Sidak correction to correct for multiple comparisons.

Post-hoc group differences on all diffusion outcome measures were performed using the general linear model (GLM) tool implemented in FSL. Age and gender were included as covariates in all statistical designs. FSL-randomise was used for voxel-wise non-permutation testing with 5000 permutations.[23] The Threshold-Free Cluster Enhancement technique was used, and family wise error was used to correct for multiple comparisons across voxels.[24]

Group differences for all VEP outcome measures were analyzed using Kruskal-Wallis test. If this analysis yielded significant results, post-hoc analysis was performed using the Mann-Whitney U test.

Separate univariate linear regression analyses were performed in HD gene carriers (i.e. both premanifest and manifest HD) to assess the associations between diffusion outcome measures and clinical assessments, and between neurophysiological outcome measures and clinical assessments. Only outcome measures that showed significant group differences compared to controls were included in the regression analyses. Age, gender and HD group were included as covariates and entered in one block with the predictor variable. The significant threshold was set at a p-value of < 0.05. Statistical analyses were performed using the Statistical Package for Social Sciences (SPSS for Mac, version 23, SPSS Inc.).

3. RESULTS

Demographic characteristics for each group are presented in Table 1. Premanifest HD gene carriers were younger compared to both controls and manifest HD ($F(2,55) = 10.81$, $p = 0.026$ and $p < 0.001$ respectively). Manifest HD had a higher disease burden score compared to premanifest HD ($t(37) = 4.6$, $p < 0.001$). In addition, manifest HD had more motor impairments compared to controls and premanifest HD on the UHDRS – total motor score ($F(2,55) = 48.06$, both $p < 0.001$) and UHDRS - oculomotor

score (F (2,55) = 67.00, both $p < 0.001$). Gender and CAG repeat length did not differ between groups.

To study structural integrity of the visual pathway, mean indices of diffusion parameters were measured along the anterior and posterior thalamic radiation tracts. Reduced FA (F (2,55) = 9.35, $p = 0.005$), increased RD (F (2,55) = 16.66, $p < 0.001$) and increased AD (F (2,55) = 8.61, $p = 0.001$) were found in manifest HD compared to controls (Figure 1A). No differences in diffusion parameters were observed between premanifest HD and controls.

Voxel-wise analysis showed that these reduced FA and increased RD values in manifest HD were primarily located posterior in the optic radiation and thalamus (Figure 1B). Reduced mean AD was found in the frontal lobe, particularly in the anterior limb of the internal capsule and thalamus.

All diffusivity parameters showed significant associations with clinical assessments (Table 2). The UHDRS total motor score, UHDRS oculomotor score and disease burden score all showed the strongest association with radial diffusivity, meaning that higher clinical scores were correlated with increased radial diffusivity.

To study functional integrity of the visual pathway, brain activity after visual stimulation

TABLE 1 Demographic group characteristics

	Controls	Premanifest HD	Manifest HD
N	17	21	20
Age (years)	46.5 ± 10.9 (24.1 – 61.3)	37.4 ± 9.0 (23.2 – 52.9)	52.1 ± 10.8 (28.5 – 64.8)
Gender (m/f)	7/10	11/10	11/9
CAG repeat length	–	41.8± 2.2 (38 – 45)	42.8 ± 2.4 (40 – 48)
Disease burden score	–	228.6 ± 88.1 (89.9 – 368.0)	362.4 ± 93.1 (185.0 – 538.8)
UHDRS – Total motor score	1.8 ± 1.3 (0 – 5)	2.8 ± 1.0 (1 – 5)	27.2 ± 15.5 (8 – 52)
UHDRS - Oculomotor	0.4 ± 0.7 (0 – 2)	1.6 ± 1.1 (0 – 4)	8.4 ± 3.7 (3 – 15)

Demographic data are showed (mean ± SD (range), except for gender (numbers)).
Disease burden score was calculated with the formula: age x [CAG repeat length – 35.5] by Penney et al., 1997.
CAG = cytosine-adenosine-guanine, UHDRS = Unified Huntington's Disease Rating Scale.

TABLE 2 Correlations between diffusion parameters and clinical assessments in HD gene carriers

	Fractional anisotropy			Axial diffusivity			Radial diffusivity		
	R^2	β_{std}	*p*-value	R^2	β_{std}	*p*-value	R^2	β_{std}	*p*-value
UHDRS – Total Motor	0.426	-0.517	**0.012**	0.374	0.605	**0.005**	0.534	0.634	**0.001**
UHDRS – Oculomotor	0.403	-0.486	**0.027**	0.316	0.501	**0.033**	0.474	0.535	**0.010**
Disease burden score	0.484	-0.585	**0.001**	0.347	0.454	**0.012**	0.583	0.620	**< 0.001**

Separate univariate linear regression analyses were performed adjusted for age, gender and HD group (i.e. premanifest and manifest HD). Standardized Beta coefficients (β_{std}) represent the SD change in diffusion parameters per every SD increase in the clinical assessments. As age is already included in the disease burden score (age x [CAG repeat length – 35.5] by Penney et al., 1997), these regression analyses were performed without age as covariate. Significant *p*-values < 0.05 are presented in bold.

FIGURE 1 Diffusion parameters

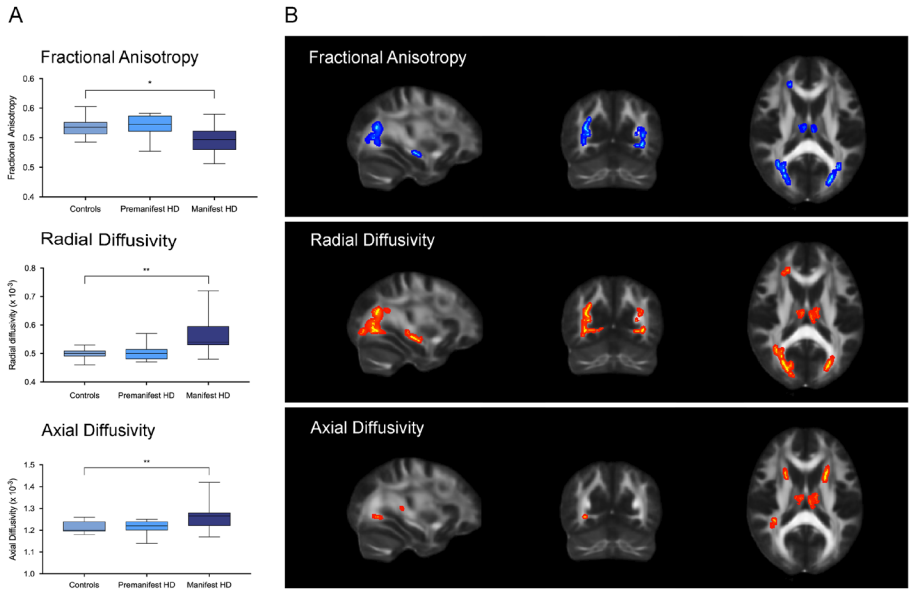

Diffusion parameters measured using tract-based spatial statistics (TBSS) analysis showed microstructural changes in manifest HD. A) Fractional anisotropy (FA), radial diffusivity (RD), and axial diffusivity (AD) values within the anterior and posterior thalamic radiation tracts are presented per group. Significant differences between manifest HD and controls are displayed, * $p < 0.05$ and ** $p \leq 0.001$. B) Voxel-based brain regions that showed significant differences in diffusion parameters between manifest HD and controls. Blue: decreased diffusivity in manifest HD compared to controls. Red: increased diffusivity in manifest HD compared to controls. Age and gender were included as covariates in the statistical model. Regions are overlaid on sagittal, coronal, and transversal slices of a standard FMRIB FA image. A family wise error corrected threshold of $p < 0.05$ was used.

was analyzed, using mean peak latencies and amplitudes of four major pattern-reversal VEP components (Figure 2 and Table 3). Four patients with HD had no recognizable signal due to motion artifacts and were therefore not included in the analyses. Significant lower peak amplitudes of the N75 and P200 components, and reduced N75-P100 peak-to-peak amplitude were found in manifest HD compared to controls (U = 206, p = 0.011; U = 37, p = 0.025; and U = 65, p = 0.010 respectively). In addition, the P200 component was also reduced in premanifest HD compared to controls (U = 66, p = 0.014). There were no significant differences between groups in mean peak latencies for any component. In addition, there were no significant associations between N75 and P200 amplitudes and clinical outcome measures (Table 4).

FIGURE 2 Visual evoked potentials

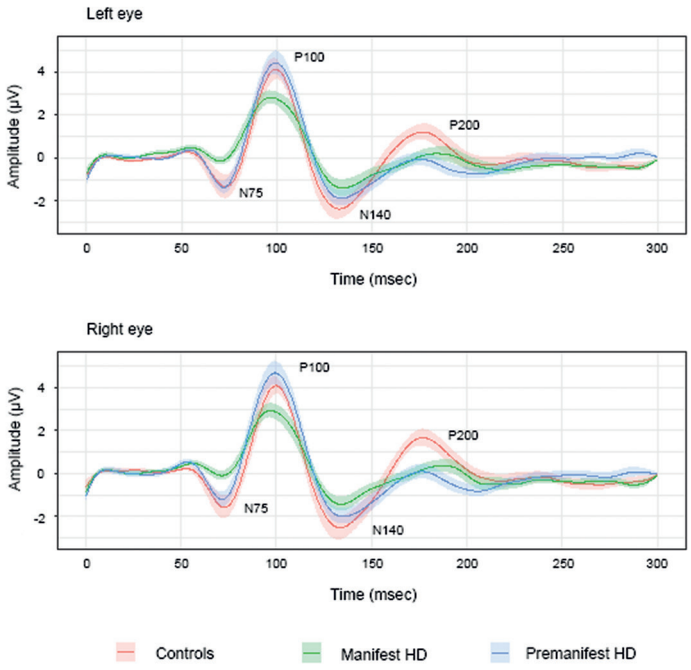

Mean pattern reversal visual evoked potentials per group measured from electrode Oz after left and right eye stimulation separately. In the manifest HD group, four participants had no recognizable signal due to motions artifacts and were not included in further analyses. The four major components, N75, P100, N140, and P200 are displayed, showing significant decreased N75 and P200 amplitudes in manifest HD compared to controls and significant decreased P200 amplitude in premanifest HD compared to controls.

TABLE 3 Mean latencies and amplitudes of pattern-reversal VEP

	Peak latency (msec)				Peak amplitude (mV)				Peak-to-peak amplitude (mV)		
	N75	P100	N140	P200	N75	P100	N140	P200	N75-P100	P100-N140	N140-P200
Controls	75.2 ± 5.9 (65.3 – 85.4)	99.9 ± 5.7 (86.9 – 110.2)	132.5 ± 6.1 (123.2 – 142.5)	171.6 ± 11.8 (142.4 – 186.3)	-2.3 ± 2.2 (-8.3 – 0.7)	4.7 ± 2.0 (1.5 – 10.5)	-3.1 ± 2.5 (-8.0 – -0.2)	2.3 ± 1.4 (0.5 – 4.2)	7.0 ± 3.4 (1.6 – 14.0)	7.7 ± 3.9 (3.1 – 18.4)	5.5 ± 3.0 (1.5 – 10.4)
Pre-HD	73.9 ± 4.8 (66.4 – 86.0)	99.2 ± 6.1 (90.1 – 116.0)	134.4 ± 9.8 (121.7 – 158.9)	175.1 ± 14.5 (151.1 – 200.3)	-1.9 ± 1.6 (-4.8 -1.0)	5.3 ± 2.5 (1.7 – 12.2)	-2.7 ± 1.6 (-5.3 – -0.0)	**0.9 ± 1.3** (-2.3 – 3.0)	7.0 ± 3.6 (2.0 – 17.0)	8.1 ± 3.7 (2.9 – 16.6)	3.7 ± 1.7 (1.0 – 6.8)
Mani-HD	74.3 ± 4.6 (67.1 – 81.3)	101.0 ± 6.8 (90.5 – 112.1)	137.0 ± 10.3 (122.0 – 159.2)	169.2 ± 16.4 (143.4 – 193.8)	**-0.7 ± 0.9** (-2.5 – 0.5)	3.9 ± 1.5 (2.2 – 6.9)	-2.4 ± 1.3 (-6.1 – -1.0)	**1.1 ± 1.3** (-0.1 – 3.6)	**4.5 ± 1.7** (2.1 – 8.5)	6.3 ± 1.8 (4.0 – 9.7)	3.7 ± 2.5 (1.1 – 9.6)

Neurophysiological data are showed (mean ± SD (range)) measured from electrode Oz. Left and right eyes were averaged for each outcome measure.
Significant differences compared to controls are displayed in bold ($p < 0.05$).

TABLE 4 Correlations between visual evoked potentials and clinical assessments in HD gene carriers

	N75 amplitude			P200 amplitude			N75-P100 amplitude		
	R^2	β_{std}	*p*-value	R^2	β_{std}	*p*-value	R^2	β_{std}	*p*-value
UHDRS – Total Motor	0.199	-0.154	0.527	0.256	0.154	0.557	0.191	-0.219	0.345
UHDRS – Oculomotor	0.189	-0.352	0.212	0.246	-0.035	0.896	0.295	-0.290	0.223
Disease burden score	0.159	0.001	0.999	0.163	0.280	0.191	0.209	-0.271	0.165

Separate univariate linear regression analyses were performed adjusted for age, gender and HD group (i.e. premanifest and manifest HD). Standardized Beta coefficients (β_{std}) represent the SD change in amplitude per every SD increase in the clinical assessments. As age is already included in the disease burden score (age x [CAG repeat length – 35.5] by Penney et al., 1997), these regression analyses were performed without age as covariate.

4. DISCUSSION

This study revealed alterations in structural and functional integrity of the visual pathway in manifest HD compared to controls. Altered microstructure was primarily present in the optic radiations of posterior brain regions and to a lesser extent in the anterior brain regions. In addition, reduced amplitudes with normal latencies were observed in response to visual stimulation using pattern-reversal visual evoked potentials as a measure of functional integrity.

Diffusion markers are thought to reflect the structural integrity of neural tracts in the brain by detecting the extent and coherence of water diffusion.[25,26] Our diffusion tensor imaging analyses showed reduced axial diffusivity (i.e., axonal degeneration) in manifest HD compared to controls in the anterior limb of the internal capsule in the frontal lobe. In contrast, reduced fractional anisotropy (i.e., overall fiber density) and increased radial diffusivity (i.e. axonal myelination and diameter) were observed more widespread in fibers located in the thalamus and optic radiations in the occipital lobe. Our findings suggest that neurodegeneration of the visual pathway predominantly occurs in fibers that project to the posterior cerebral cortex due to loss of axonal fibers, which is in line with postmortem studies that observed neuronal cell loss and a reduction of axonal connections in the occipital lobe.[8,9]

Microstructural changes in tracts to the prefrontal cortex, sensorimotor cortex and corpus callosum were found in previous studies that assessed cortico-striatal and deep white matter pathways across the entire brain in patients with HD.[27] Diffusivity changes of posterior cerebral tracts have also been found in HD, particularly located in the frontal white matter projections to the occipital lobe.[28–30] In these studies, however, alterations in the occipital cortex have not been the primary focus of interest.

Although striatal atrophy can be detected in premanifest HD a decade before the onset of motor symptoms,[5] we did not detect microstructural white matter changes in our group of premanifest HD gene carriers. It is possible that axonal loss in the white matter tracts to the cortex only occurs in manifest disease stages and that microstructural changes during premanifest stages are more variable and dynamic over time.[31] In contrast, a longitudinal study did observe changes in diffusivity over time in the fronto-occipital tracts in premanifest HD, most prominently in the individuals close to estimated disease onset.[28] However, the premanifest HD group in this study already showed motor symptoms, suggesting that the distinction between manifest and premanifest was based on different criteria than our study, making direct comparisons difficult.

We additionally examined correlations between clinical functional assessments and diffusion outcome measures. The strongest association was found between disease burden score and radial diffusivity, indicating that higher disease severity is correlated with increased axonal fiber loss. This finding suggests that diffusion measurements within the visual pathway can be used as a marker of disease severity.

While diffusion markers reflect the structural integrity of white matter tracts, visual-evoked potentials are frequently used to measure the functional integrity of the retinal-cortical pathway. The neural generators of the main components of the evoked potential wave (before 150 milliseconds) are considered to originate in the primary visual cortex, while late components (after 150 milliseconds) reflect activity in the associative occipital and parietal cortical areas.[32] In our study, normal latencies of both main and late components were observed in HD gene carriers, which imply preserved pre-chiasmatic function and normal conduction velocities to the primary cortex in early disease stages, since prolonged latencies are generally found in demyelination disorders.[33] We did observe reduced amplitudes for both main and late components (N75 and P200 respectively) in manifest HD compared to controls. Therefore, in addition to our findings of altered structural integrity, we provide evidence of changed functional integrity in the optic tracts in patients with HD as well. There are no previous studies that examined both visual-evoked potentials and microstructural brain changes of the visual pathway in HD. In line with our findings, several previous neurophysiological studies also reported reduced amplitudes in HD patients with normal latencies of the main components in response to light flashes or checkerboard pattern-reversal stimulation.[34–37] Other pattern-reversal VEP studies, however, report no significant differences in both amplitudes and latencies of the main components in manifest HD compared to controls.[38,39] Nonetheless, these studies were conducted before genetic testing became available and different criteria were used to define patients with HD. Recent neurophysiological studies focused on the late components to investigate higher level visual processing using more challenging visual processing tasks, such as a word recognition task,[40] attentional categorization tasks,[41,42] or a facial emotion expression task.[37] These studies all found reduced amplitudes for late components.[37,41,42] Since reduced main component amplitudes are frequently reported in manifest HD, it is hypothesized that early visual processing is already impaired, thus making subsequent visual processing more difficult.[37] We did observe reduced amplitudes in main and late components in manifest HD, but future studies with a larger sample size and different stimulation types could elucidate this hypothesis more thoroughly.

In our study, reduced amplitudes in premanifest HD gene carriers were additionally observed for the late component (P200). Only two other studies assessed the response to visual-evoked potentials in premanifest HD gene carriers, before the onset of overt motor symptoms.[41,42] One study also observed reduced amplitudes of the late component in premanifest HD in response to a visual attentional processing task, while another study did not find neurophysiological impairments in early perceptual processing in premanifest HD.[41,42] As the latter study involved more complex stimulation tasks, a direct comparison to our pattern-reversal VEP is not possible.

We did not observe a significant relationship between neurophysiological measures and clinical assessments in HD gene carriers, possibly because of the heterogeneity seen in the waveforms of all participants or the effects of gender and age on evoked-potential components.[43] To address the issue of heterogeneity of VEP responses, longitudinal studies could be performed with larger sample sizes to measure individual change over time as a marker for disease progression.

This study examined the microstructure of regional white matter tracts of the visual pathway and the response on pattern-reversal visual-evoked potentials in premanifest and manifest HD gene carriers.

In conclusion, changes in structural integrity were most prominently present in the thalamus and optic radiations in early manifest HD, and were associated with functional scores, such as disease burden and oculomotor scores, suggesting that microstructural changes in the optic tracts are related with clinical disease severity. In addition, reduced amplitudes with normal latencies were observed in response to visual stimulation in manifest HD patients.

Our findings show that the posterior brain regions undergo structural alterations in early stages of the neuropathological process in HD. These data provide more knowledge on the pathophysiological processes in the cerebral cortex and might aid in the identification of other regions than the striatum that can be used as a potential marker of disease severity for future clinical trials.

REFERENCES

1. Bates GP, Dorsey R, Gusella JF, et al. Huntington disease. *Nat Rev Dis Prim*. 2015;1:1-21.
2. The Huntington's Disease Collaborative Research Group. A novel gene containing a trinucleotide repeat that is expanded and unstable on Huntington's disease chromosomes. *Cell*. 1993;72(6):971-983.
3. Vonsattel JP, Myers RH, Stevens TJ, Ferrante RJ, Bird ED, Richardson EP. Neuropathological classification of Huntington's disease. *J Neuropathol Exp Neurol*. 1985;44(6):559-577.
4. Reiner A, Albin RL, Anderson KD, D'Amato CJ, Penney JB, Young AB. Differential loss of striatal projection neurons in Huntington disease. *Proc Natl Acad Sci U S A*. 1988;85(15):5733-5737.
5. Aylward E, Sparks B, Field K, et al. Onset and rate of striatal atrophy in preclinical Huntington disease. *Neurology*. 2004;63:66-72.
6. Tabrizi SJ, Scahill RI, Owen G, et al. Predictors of phenotypic progression and disease onset in premanifest and early-stage Huntington's disease in the TRACK-HD study: Analysis of 36-month observational data. *Lancet Neurol*. 2013;12(7):637-649.
7. Coppen EM, van der Grond J, Hart EP, Lakke EAJF, Roos RAC. The visual cortex and visual cognition in Huntington's disease: An overview of current literature. *Behav Brain Res*. 2018;351:63-74.
8. Rüb U, Seidel K, Vonsattel JP, et al. Huntington's disease (HD): Neurodegeneration of Brodmann's primary visual area 17 (BA17). *Brain Pathol*. 2015;25(6):701-711.
9. Nana AL, Kim EH, Thu DCV, et al. Widespread heterogeneous neuronal loss across the cerebral cortex in Huntington's disease. *J Huntingtons Dis*. 2014;3:45-64.
10. Lange H. Quantitative changes of telencephalon, diencephalon, and mesencephalon in Huntington's chorea, postencephalitic, and idiopathic parkinsonism. *Verh Anat Ges*. 1981;75:923-925.
11. Johnson EB, Rees EM, Labuschagne I, et al. The impact of occipital lobe cortical thickness on cognitive task performance: An investigation in Huntington's Disease. *Neuropsychologia*. 2015;79:138-146.
12. Coppen EM, Jacobs M, van den Berg-huysmans AA, van der Grond J, Roos RAC. Grey matter volume loss is associated with specific clinical motor signs in Huntington's disease. *Park Relat Disord*. 2018;46:56-61.
13. Tabrizi SJ, Langbehn DR, Leavitt BR, et al. Biological and clinical manifestations of Huntington's disease in the longitudinal TRACK-HD study: cross-sectional analysis of baseline data. *Lancet Neurol*. 2009;8(9):791-801.

14. Coppen EM, van der Grond J, Hafkemeijer A, Rombouts SARB, Roos RAC. Early grey matter changes in structural covariance networks in Huntington's disease. *NeuroImage Clin*. 2016;12:806-814.
15. Rosas HD, Salat DH, Lee SY, et al. Cerebral cortex and the clinical expression of Huntington's disease: complexity and heterogeneity. *Brain*. 2008;131(4):1057-1068.
16. Huntington Study Group. Unified Huntington's disease rating scale: reliability and consistency. *Mov Disord*. 1996;11(2):136-142.
17. Marder K, Zhao H, Myers RH, et al. Rate of functional decline in Huntington's disease. *Neurology*. 2000;54:452-458.
18. Penney J, Vonsattel JP, MacDonald ME, Gusella JF, Myers RH. CAG repeat number governs the development rate of pathology in Huntington's disease. *Ann Neurol*. 1997;41(5):689-692.
19. Smith SM, Jenkinson M, Woolrich MW, et al. Advances in functional and structural MR image analysis and implementation as FSL. *Neuroimage*. 2004;23:S208-S219.
20. Behrens TEJ, Woolrich MW, Jenkinson M, et al. Characterization and propagation of uncertainty in diffusion-weighted MR imaging. *Magn Reson Med*. 2003;50(5):1077-1088.
21. Smith SM, Jenkinson M, Johansen-Berg H, et al. Tract-based spatial statistics: voxelwise analysis of multi-subject diffusion data. *Neuroimage*. 2006;31(4):1487-1505.
22. Vernon Odom J, Bach M, Brigell M, et al. ISCEV standard for clinical visual evoked potentials: (2016 update). *Doc Ophthalmol*. 2016;133:1-9.
23. Winkler AM, Ridgway GR, Webster MA, Smith SM, Nichols TE. Permutation inference for the general linear model. *Neuroimage*. 2014;92:381-397.
24. Smith SM, Nichols TE. Threshold-free cluster enhancement: addressing problems of smoothing, threshold dependence and localisation in cluster inference. *Neuroimage*. 2009;44(1):83-98.
25. Rees EM, Scahill RI, Hobbs NZ. Longitudinal neuroimaging biomarkers in Huntington's disease. *J Huntingtons Dis*. 2013;2:21-39.
26. Alexander AL, Lee JE, Lazar M, Field AS. Diffusion Tensor Imaging of the Brain. *Neurotherapeutics*. 2007;4(3):316-329.
27. Liu W, Yang J, Burgunder JM, Cheng B, Shang H. Diffusion imaging studies of Huntington's disease: A meta-analysis. *Park Relat Disord*. 2016;32:94-101.
28. Harrington DL, Long JD, Durgerian S, et al. Cross-sectional and longitudinal multimodal structural imaging in prodromal Huntington's disease. *Mov Disord*. 2016;31(11):1664-1675.
29. Matsui JT, Vaidya JG, Wassermann D, et al. Prefrontal cortex white matter tracts in prodromal Huntington disease. *Hum Brain Mapp*. 2015;36(10):3717-3732.
30. Faria AV, Ratnanather JT, Tward DJ, et al. Linking white matter and deep gray matter alterations in premanifest Huntington disease. *NeuroImage Clin*. 2016;11:450-460.
31. Poudel GR, Stout JC, Domínguez D. JF, et al. Longitudinal change in white matter microstructure in Huntington's disease: The IMAGE-HD study. *Neurobiol Dis*. 2015;74:406-412.

32. Di Russo F, Pitzalis S, Spitoni G, et al. Identification of the neural sources of the pattern-reversal VEP. *Neuroimage*. 2005;24(3):874-886.
33. Brecelj J. Visual electrophysiology in the clinical evaluation of optic neuritis, chiasmal tumours, achiasmia, and ocular albinism: an overview. *Doc Ophthalmol*. 2014;129:71-84.
34. Ellenberger C, Petro DJ, Ziegler SB. The visuallly evoked potential in Huntington Disease. *Neurology*. 1978;28:95-97.
35. Josiassen R, Shagass C, Mancall E, Roemer R. Auditory and visual evoked potentials in Huntington's disease. *Electroencephalogr Clin Neurophysiol*. 1984;57:113-118.
36. Oepen G, Doerr M, Thoden U. Visual (VEP) and somatosensory (SSEP) evoked potentials in Huntington's chorea. *Electroencephalogr Clin Neurophysiol*. 1981;51:666-670.
37. Croft RJ, McKernan F, Gray M, Churchyard A, Georgiou-Karistianis N. Emotion perception and electrophysiological correlates in Huntington's disease. *Clin Neurophysiol*. 2014;125(8):1618-1625.
38. Ehle AL, Stewart RM, Lellelid NA, Leventhal NA. Evoked potentials in Huntington's disease. A comparative and longitudinal study. *Arch Neurol*. 1984;41(4):379-382.
39. Rosenberg C, Nudleman K, Starr A. Cognitive evoked potentials (P300) in early Huntington's disease. *Arch Neurol*. 1985;42(10):984-987.
40. Munte TF, Ridao-Alonso ME, Preinfalk J, et al. An electrophysiological analysis of altered cognitive functions in Huntington Disease. *Arch Neurol*. 1997;54:1089-1098.
41. Antal A, Beniczky S, Kincses TZ, Jakab K, Benedek G, Vecsei L. Perceptual categorization is impaired in Huntington's disease: An electrophysiological study. *Dement Geriatr Cogn Disord*. 2003;16(4):187-192.
42. Beste C, Saft C, Andrich J, Gold R, Falkenstein M. Stimulus-response compatibility in Huntington's disease: A cognitive-neurophysiological analysis. *J Neurophysiol*. 2008;99:1213-1223.
43. de Freitas Dotto P, Berezovsky A, Sacai PY, Rocha DM, Salomão SR. Gender-based normative values for pattern-reversal and flash visually evoked potentials under binocular and monocular stimulation in healthy adults. *Doc Ophthalmol*. 2017;135:53-67.

7